Spin-orbit torque driven by a planar Hall current

Christopher Safranski^{1,2}, Eric A. Montoya D^{1,2} and Ilya N. Krivorotov D^{1*}

Spin-orbit torques (SOTs) in multilayers of ferromagnetic (FM) and non-magnetic (NM) metals can manipulate the magnetization of the FM layer efficiently. This is employed, for example, in non-volatile magnetic memories for energyefficient mobile electronics^{1,2} and spin torque nano-oscillators³⁻⁷ for neuromorphic computing⁸. Recently, spin torque nano-oscillators also found use in microwave-assisted magnetic recording, which enables ultrahigh-capacity hard disk drives9. Most SOT devices employ spin Hall10,11 and Rashba12 effects, which originate from spin-orbit coupling within the NM layer and at the FM/NM interfaces, respectively. Recently, SOTs generated by the anomalous Hall effect in FM/NM/FM multilayers were predicted¹³ and experimentally realized14. The control of SOTs through crystal symmetry was demonstrated as well¹⁵. Understanding all the types of SOTs that can arise in magnetic multilayers is needed for a formulation of a comprehensive SOT theory and for engineering practical SOT devices. Here we show that a spin-polarized electric current known to give rise to anisotropic magnetoresistance (AMR) and the planar Hall effect (PHE) in a FM¹⁶ can additionally generate large antidamping SOTs with an unusual angular symmetry in NM₁/FM/NM₂ multilayers. This effect can be described by a recently proposed magnonic mechanism¹⁷. Our measurements reveal that this torque can be large in multilayers in which both spin Hall and Rashba torques are negligible. Furthermore, we demonstrate the operation of a spin torque nano-oscillator driven by this SOT. These findings significantly expand the class of materials that exhibit giant SOTs.

We measured SOTs in substrate/NM₁/FM/NM₂ nanowire devices (Methods), shown in Fig. 1a, along with the coordinate system used in this letter. Ta/Au, Ta/Pt and Ta/Pd bilayers were chosen as NM₁, and Ta, Au/Ta and Au/AlO_x were employed as NM₂ (Supplementary Notes 1 and 2). We used a [Co(0.85 nm)/Ni(1.28 nm)]₂/Co(0.85 nm) superlattice as the FM layer to take advantage of the perpendicular magnetic anisotropy in this system^{18,19} that nearly cancels the demagnetizing field of the FM film. The AMR curves shown in Fig. 1b demonstrate that the magnetization of the Ta(3 nm)/Au(3.9 nm)/FM/Ta(4 nm) nanowire easily saturates for both the in-plane and out-of-plane magnetic fields.

We characterized the SOTs by field-modulated spin torque ferromagnetic resonance (ST-FMR) (Methods, Supplementary Note 3 and Supplementary Fig. 2)²⁰. The ST-FMR spectra of the Ta/Au/FM/ Ta device for a magnetic field H applied in the xz plane (Fig. 1c) exhibited several spin wave resonances. Figure 1d demonstrates that the linewidths of these resonances are altered by a direct current $I_{\rm dc}$. The blue symbols in Fig. 1e show the linewidth ΔH of the lowest-frequency mode (labelled M_1) versus sheet current density $K_{\rm dc} = I_{\rm dc}/w$, where w is the nanowire width (Methods). The linewidth, proportional to the FM magnetic damping α , was found to be a linear function of $K_{\rm dc}$, which reveals the presence of a SOT in

the xz plane that can tune α (here referred to as an antidamping SOT). We also found the magnitude of the spin Hall torque (SHT) to be small in this system, as evidenced by the weak dependence of ΔH on $K_{\rm dc}$ for magnetization nearly parallel to the y axis, where the strongest antidamping effect of SHT is expected (red symbols in Fig. 1e)¹¹.

Figure 1f shows the angular dependence of the slope of ΔH as a function of $K_{\rm dc}$, which quantifies the strength of the an antidamping SOT. For magnetization that lies in the xy plane (red symbols), ${\rm d}\Delta H/{\rm d}K_{\rm dc}$ is small and is consistent with the 360° periodicity expected for SHT. In contrast, ${\rm d}\Delta H/{\rm d}K_{\rm dc}$ in the xz plane (blue symbols) is 180° periodic and is large when the magnetization makes a 45° angle with respect to the sample normal. The angular dependence of ${\rm d}\Delta H/{\rm d}K_{\rm dc}$ in Fig. 1fis fitted well by $(\hat{\bf m}\cdot\hat{\bf x})(\hat{\bf m}\cdot\hat{\bf z})=\cos(\theta)\sin(\theta)\cos(\phi)$ (blue curve), where $\hat{\bf m}$ is the unit vector in the direction of the FM magnetization.

The data in Fig. 1e show that ΔH extrapolates to zero at a critical sheet current density K_c , beyond which the FM magnetization is expected to auto-oscillate. Figure 2 shows spectra of the microwave signal generated by the sample (Methods) as a function of K_{dc} for a magnetic field applied along the four quadrant bisectors of the xz plane. The sample generates a microwave signal for one current polarity when $|K_{dc}|$ exceeds a critical value $|K_c|$. The data in Fig. 2 reveal that $K_c < 0$ for H parallel to the x=z bisectors, whereas $K_c > 0$ for H parallel to the x=z bisectors, in agreement with the ST-FMR data in Fig. 1f. Several auto-oscillatory modes are excited above K_c , with the highest-amplitude mode M_1 generating up to $60\,\mathrm{pW}$ of microwave power (Supplementary Note 4 and Supplementary Fig. 3).

To understand the effect of the NM layers on antidamping SOTs, we studied a set of NM₁/FM/Ta(4 nm) nanowires that employed different NM₁ layers with similar sheet resistances, Ta(3 nm)/Au(3.9 nm), Ta(3 nm)/Pt(7.0 nm) and Ta(3 nm)/Pd(8.0 nm) (Supplementary Note 2). The angular dependence of $d\Delta H/dK_{dc}$, which quantifies an antidamping SOT, was measured in the xy and xz planes. Figure 3a shows that the magnitude of the 360° periodic antidamping SHT in the xy plane strongly depends on the NM₁ material, in agreement with previous studies²¹. The data in Fig. 3b demonstrate that the magnitude of the 180° periodic antidamping SOT in the xz plane is similar for all three NM₁ layers. Figure 3a,b reveals that the magnitudes of SHT and the 180° periodic antidamping SOT in the xz plane are not correlated and thus the mechanisms that give rise to these SOTs are different. In Supplementary Note 5, we show that the observed 180° periodic SOT does not arise from the Rashba mechanism²².

As the existing models of SOT at FM/NM interfaces do not explain our experimental data in their entirety, a new approach is needed. We argue that the observed 180° periodic antidamping SOT in the *xz* plane arises from the planar Hall current generated by spin–orbit coupling in a FM conductor and absorbed by the adjacent NM layers, and thus this SOT can be called a planar Hall current driven spin–orbit torque (PHT). In this model,

LETTERS NATURE NANOTECHNOLOGY

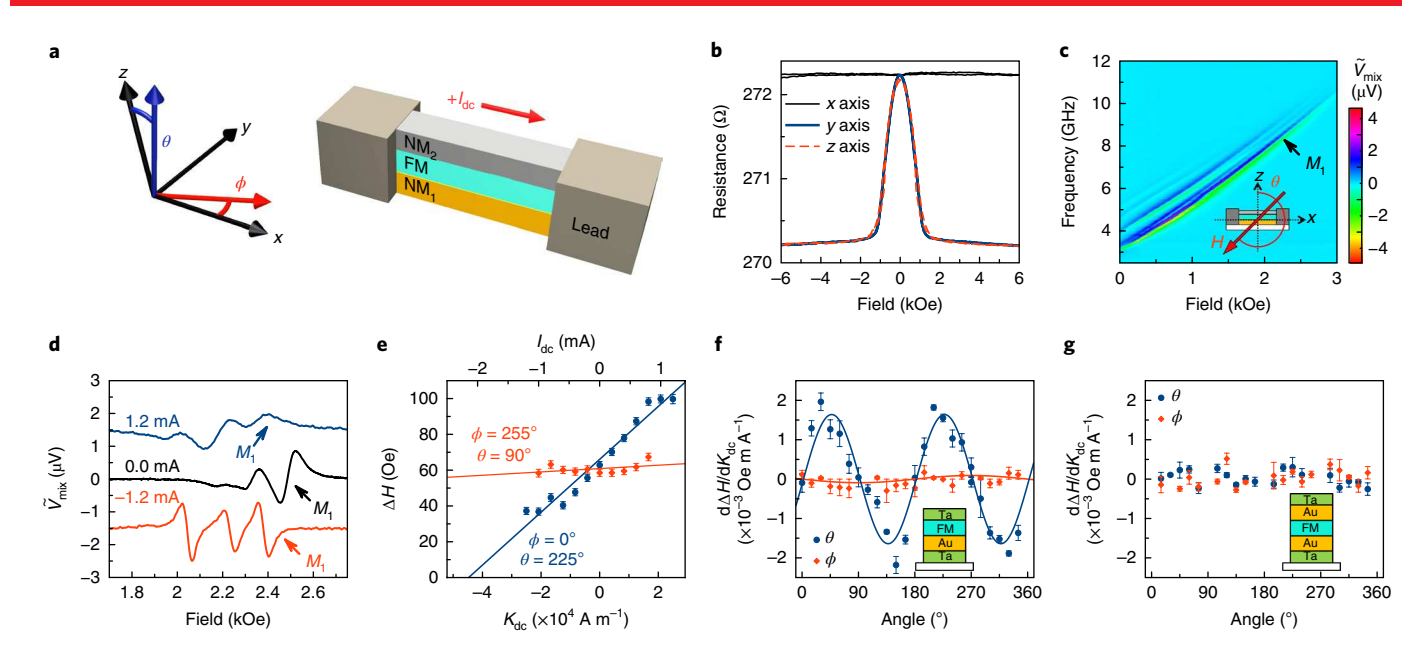


Fig. 1 | Sample geometry and ST-FMR measurements. **a**, Schematic of a NM₁/FM/NM₂ metallic nanowire device, as well as the Cartesian (x, y, z) and spherical (θ , ϕ) coordinate systems employed here. **b**, Magnetoresistance of the Ta/Au/FM/Ta device for a magnetic field applied along the principal axes. **c**, ST-FMR rectified voltage \vec{V}_{mix} as a function of frequency f and magnetic field H applied in the xz plane at θ = 225° (ϕ = 0). **d**, Effect of current bias I_{dc} on ST-FMR spectra for f = 9 GHz and θ = 225° (ϕ = 0). **e**, Linewidth ΔH of the lowest-frequency mode M_1 as a function of the sheet current density K_{dc} for magnetization in the xy (red) and xz (blue) planes (f = 9 GHz). **f**,g, Angular dependence of $d\Delta H/dK_{\text{dc}}$ in the xy (red) and xz (blue) planes for the Ta/Au/FM/Ta (**f**) and Ta/Au/FM/Au/Ta (**g**) devices. Error bars show the standard error of least squares fit (Methods). Measurements in **b-g** were made at room temperature.

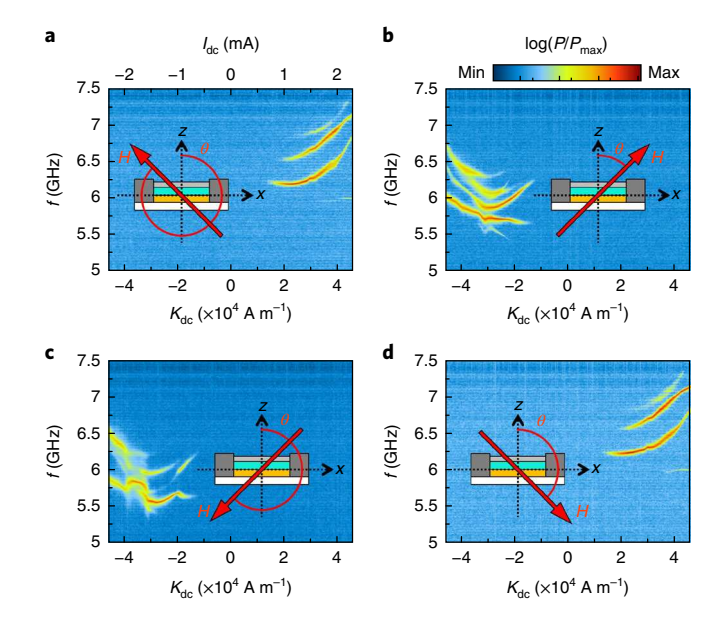


Fig. 2 | Microwave generation. Normalized power spectral P density of a microwave signal generated by the Ta/Au/FM/Ta device as a function of frequency f and applied sheet current density $K_{\rm dc}$. **a-d**, A 1.7 kOe magnetic field H is applied in the xz plane at four angles, θ =315° (**a**), θ =45° (**b**), θ =225° (**c**) and θ =135° (**d**). The insets show the side view of the device and the applied field direction. The measurements were made at T=77 K.

the antidamping SOT originates from the exchange of angular momentum between the FM and NM layers via spin currents. For this exchange to occur, the NM layer must behave as a good spin sink, that is, it must both allow the transfer of spin current across the FM/NM interface and efficiently flip spins. The PHE results in a current of spin-polarized electrons of density $J_{\text{PHF}} = \Delta \sigma_{\text{AMR}}(\hat{\mathbf{m}} \cdot \mathbf{E})\hat{\mathbf{m}}$

flowing in the FM parallel to its magnetization, where $\mathbf{E} \approx E\hat{\mathbf{x}}$ is the applied electric field and $\Delta\sigma_{\rm AMR}$ is the anisotropic part of the FM conductivity^{13,16}. Only the component of $J_{\rm PHE}$ normal to the NM/FM interface can transfer spin and contribute to the SOT:

$$J_{\text{PHE}}^{z} = \Delta \sigma_{\text{AMR}} E(\hat{\mathbf{m}} \cdot \hat{\mathbf{x}})(\hat{\mathbf{m}} \cdot \hat{\mathbf{z}})$$
 (1)

The angular dependence of $J_{\rm PHE}^z$ is identical to the measured angular dependence of the antidamping SOT in Fig. 3b. When $J_{\text{PHE}}^z < 0$, the planar Hall current drives electrons with magnetic moments aligned with the FM magnetization from the FM layer into the bottom NM₁ layer¹⁶, as shown in Fig. 3c (black ball and arrows). In a steady state, the net electron current across the NM₁/FM interface is zero, which implies a backflow of electrons from the NM₁ layer to the FM layer. The backflow current density from a NM₁ layer with strong spin-flip scattering (a good spin sink) is weakly spin polarized, which results in a net pure spin current density Q_{PHE}^{z} polarized along $\hat{\mathbf{m}}$ that flows in the $-\hat{z}$ direction across the NM₁/FM interface. A spin current may also flow across the NM₂/FM interface. If pure spin currents across the NM₁/FM and FM/NM₂ interfaces differ, a net spin transfer to the FM layer takes place. For example, our spin pumping measurements (Supplementary Note 7) reveal that $NM_1 = Ta/Au$ is a good spin sink but NM₂=Ta is a poor spin sink, which gives rise to large net-spin transfer to the FM layer in the Ta/Au/FM/Ta nanowire device and is consistent with the large value of PHT measured for this sample (Fig. 1f). The action of PHT changes from negative to positive damping under the reversal of I_{dc} , as shown in Fig. 3d, where Q_{PHE}^z now flows in the $+\hat{z}$ direction across the NM/FM interface. As Q_{PHE}^z changes sign on a 90° rotation of $\hat{\mathbf{m}}$ in the xz plane (equation (1)), the effect of PHT changes from a positive to a negative damping on such a rotation, in agreement with Figs. 1f and 2.

The spin-polarization direction $\hat{\mathbf{p}}$ of Q_{PHE}^z is collinear with $\hat{\mathbf{m}}$, and thus Q_{PHE}^z cannot give rise to the conventional SOTs proportional to $\hat{\mathbf{m}} \times \hat{\mathbf{p}}$ or $\hat{\mathbf{m}} \times (\hat{\mathbf{p}} \times \hat{\mathbf{m}})$ that are generated by the component of spin current transverse to the magnetization²². However, the

LETTERS

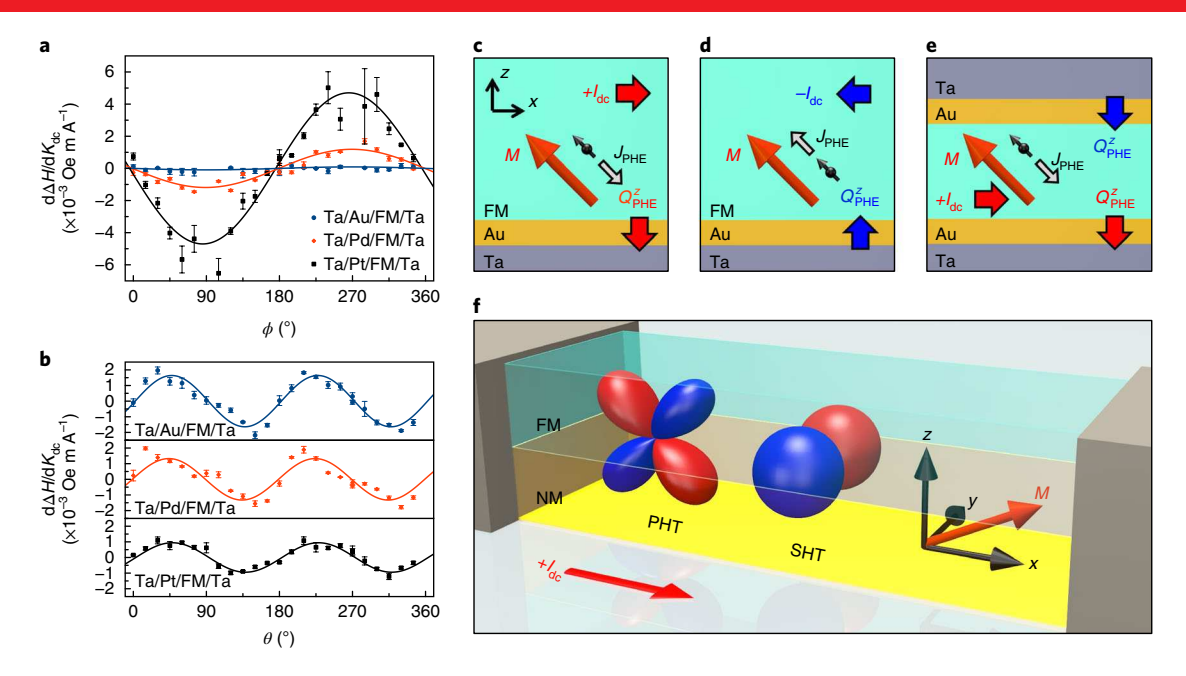


Fig. 3 | Angular symmetry and material dependence of SOTs. a,b, $d\Delta H/dK_{dc}$ measured at room temperature for different NM₁ layers characterizes the strength of the antidamping SHT in the xy plane (a) and that of the antidamping PHT in the xz plane (b). c-e, Schematics of the flow of pure spin current Q_{pHE}^{T} deriven across the NM/FM interface by spin-polarized planar Hall current density J_{PHE} in the FM layer for $I_{dc} > 0$ (c) and $I_{dc} < 0$ (d) in the Ta/Au/FM/Ta device and for $I_{dc} > 0$ in the Ta/Au/FM/Au/Ta device (e). The red and blue arrows labelled $\pm I_{dc}$ show the direction of the electric current I_{dc} applied to the nanowire. The red arrows labelled M show the direction of magnetization. The black ball and arrows represent an electron of J_{PHE} and its spin polarization. The grey arrows show the direction of J_{PHE} . f, Schematic of the angular dependence of antidamping SOTs at a NM/FM interface, biaxial PHT and uniaxial SHT. Here red (blue) corresponds to negative (positive) damping when $I_{dc} > 0$. Error bars show the standard error of least squares fit (Methods).

absorption of a longitudinal spin current $(\hat{\mathbf{p}}||\hat{\mathbf{m}})$ by the FM can give rise to an antidamping torque. An example of such a mechanism is the magnonic torque initially discussed and demonstrated in the context of the spin Seebeck torque in FM/NM bilayers^{17,23}. In this mechanism, electrons that carry a longitudinal spin current across the FM/NM interface undergo inelastic spin-flip scattering either in the FM or at the FM/NM interface and thereby generate magnons in the FM. Rapid magnon-magnon relaxation processes within the non-equilibrium cloud of magnons created by the longitudinal spin current transfer the injected angular momentum from high-energy magnons to the low-energy spin wave modes and thereby reduce the damping of these modes¹⁷. Recent spectroscopic measurements directly confirmed the generation of a non-equilibrium magnon cloud by the injection of spin currents into a FM as well as by a rapid relaxation of the injected angular momentum to the low-energy spin waves that exhibit a current-induced damping reduction^{24,25}. Further theoretical work is needed for a quantitative understanding of the antidamping torque that arises from the planar Hall current.

The PHT model not only predicts the correct angular dependence of the observed antidamping SOT, but also explains the effect of the NM material on the SOT magnitude. For a given FM layer, the PHT magnitude is controlled by the degree of spin polarization of the backflow current from the NM layer into the FM layer. Our spin pumping measurements (Supplementary Note 7) show that Ta/Au, Ta/Pd and Ta/Pt are good spin sinks and thus generate weakly spin-polarized backflow currents, which leads to similar magnitudes of PHT in all three multilayers shown in Fig. 3b. The PHT model also explains the large differences in the antidamping SOT magnitude observed for multilayers with identical top and bottom FM/NM interfaces, for example, the Ta/Au/FM/Au/AlO_x system exhibits a large antidamping SOT (Supplementary Note 6), whereas SOT in the Ta/Au/FM/Au/Ta multilayer is zero (Fig. 1g). As $NM_1 = Au/Ta$ is a good spin sink, equally large spin currents $Q_{\rm PHE}^{z}$ flow across the top and bottom Au/FM interfaces in the Ta/Au/FM/Au/Ta nanowire, which results in a zero

net angular momentum transfer to the FM and zero PHT, as illustrated in Fig. 3e. In contrast, we found that $\operatorname{Au/AlO}_x$ is a poor spin sink and thus $Q_{\rm PHE}^z$ across the FM/Au top interface is nearly zero while the $Q_{\rm PHE}^z$ across the Au/FM bottom interface is large, which results in significant angular momentum transfer to the FM and strong PHT in the Ta/Au/FM/Au/AlO $_x$ system. The angular dependences of the antidamping PHT $(\hat{\mathbf{m}} \cdot \hat{\mathbf{x}})(\hat{\mathbf{m}} \cdot \hat{\mathbf{z}})$ and SHT $(\hat{\mathbf{m}} \cdot \hat{\mathbf{y}})$ are shown in Fig. 3f, where the biaxial angular symmetry of PHT is apparent.

It is expected from equation (1) that the magnitude of PHT is proportional to the magnitude of AMR in the FM layer. We found that the AMR ratio in our Ta/Au/FM/Ta multilayer increased by a factor of 1.8 on cooling the sample from 295 K to 77 K (Supplementary Note 8 and Supplementary Fig. 7). At the same time, the critical sheet current density K_c decreased by a factor of 1.8 (from -4.4×10^4 A m⁻¹ at 295 K to -2.5×10^4 A m⁻¹ at 77 K, as measured by ST-FMR at 9 GHz (Supplementary Fig. 7). As K_c is inversely proportional to the PHT magnitude, these data support the proportionality of PHT and AMR. Furthermore, the analysis in Supplementary Note 9 reveals that the measured absolute value of PHT is consistent with that expected from the measured absolute value of AMR.

Recently, SOTs that arise from planar and anomalous Hall effects were predicted in FM/NM/FM trilayers, where the planar and anomalous Hall currents generated in one FM apply spin transfer torques to magnetization of the other FM¹³. Experiments show that current-driven coupling between two FM layers in a FM/NM/FM trilayer can be achieved via SOTs generated at the NM/FM interfaces^{26,27}. Our work reveals that a strong antidamping SOT that originates from planar Hall current in the FM layer and acts on magnetization of the same FM layer can arise in a NM/FM/NM multilayer when the efficiency of the spin transfer at one of the NM/FM interfaces is large and the NM is a good spin sink. We expect this SOT to play a significant role in the spin torque switching of magnetization²⁸ as well as in current-driven domain wall²⁹ and skyrmion³⁰ motion in magnetic multilayers.

LETTERS NATURE NANOTECHNOLOGY

Online content

Any methods, additional references, Nature Research reporting summaries, source data, statements of data availability and associated accession codes are available at https://doi.org/10.1038/s41565-018-0282-0.

Received: 2 February 2018; Accepted: 19 September 2018; Published online: 29 October 2018

References

- Miron, I. M. et al. Perpendicular switching of a single ferromagnetic layer induced by in-plane current injection. *Nature* 476, 189–193 (2011).
- Liu, L. et al. Spin-torque switching with the giant spin Hall effect of tantalum. Science 336, 555–558 (2012).
- Slavin, A. & Tiberkevich, V. Nonlinear auto-oscillator theory of microwave generation by spin-polarized current. IEEE Trans. Magn. 45, 1875–1918 (2009).
- 4. Demidov, V. E. et al. Magnetic nano-oscillator driven by pure spin current. *Nat. Mater.* **11**, 1028–1031 (2012).
- Duan, Z. et al. Nanowire spin torque oscillator driven by spin orbit torques. Nat. Commun. 5, 5616 (2014).
- Collet, M. et al. Generation of coherent spin-wave modes in yttrium iron garnet microdiscs by spin-orbit torque. Nat. Commun. 7, 10377 (2016).
- Awad, A. A. et al. Long-range mutual synchronization of spin Hall nano-oscillators. *Nat. Phys.* 13, 292–299 (2016).
- 8. Torrejon, J. et al. Neuromorphic computing with nanoscale spintronic oscillators. *Nature* **547**, 428–431 (2017).
- Western Digital unveils next-generation technology to preserve and access the next decade of big data (Western Digital, 2017); https://www.wdc.com/ about-wd/newsroom/press-room/2017-10-11-western-digital-unveils-nextgeneration-technology-to-preserve-and-access-the-next-decade-of-big-data.html
- Ando, K. et al. Electric manipulation of spin relaxation using the spin Hall effect. Phys. Rev. Lett. 101, 036601 (2008).
- 11. Sinova, J., Valenzuela, S. O., Wunderlich, J., Back, C. H. & Jungwirth, T. Spin Hall effects. *Rev. Mod. Phys.* 87, 1213–1260 (2015).
- 12. Manchon, A., Koo, H. C., Nitta, J., Frolov, S. M. & Duine, R. A. New perspectives for Rashba spin-orbit coupling. *Nat. Mater.* **14**, 871–882 (2015).
- Taniguchi, T., Grollier, J. & Stiles, M. D. Spin-transfer torques generated by the anomalous Hall effect and anisotropic magnetoresistance. *Phys. Rev. Appl.* 3, 044001 (2015).
- Gibbons, J. D., MacNeill, D., Buhrman, R. A. & Ralph, D. C. Reorientable spin direction for spin current produced by the anomalous Hall effect. *Phys. Rev. Appl.* 9, 064033 (2018).
- MacNeill, D. et al. Control of spin-orbit torques through crystal symmetry in WTe₂/ferromagnet bilayers. Nat. Phys. 13, 300-305 (2016).
- Kokado, S., Tsunoda, M., Harigaya, K. & Sakuma, A. Anisotropic magnetoresistance effects in Fe, Co, Ni, Fe₄N, and half-metallic ferromagnet: a systematic analysis. J. Phys. Soc. Jpn 81, 024705 (2012).
- Bender, S. A. & Tserkovnyak, Y. Thermally driven spin torques in layered magnetic insulators. *Phys. Rev. B* 93, 064418 (2016).
- Mangin, S. et al. Current-induced magnetization reversal in nanopillars with perpendicular anisotropy. Nat. Mater. 5, 210–215 (2006).
- Arora, M., Hübner, R., Suess, D., Heinrich, B. & Girt, E. Origin of perpendicular magnetic anisotropy in Co/Ni multilayers. *Phys. Rev. B* 96, 024401 (2017).
- Gonçalves, A. M. et al. Spin torque ferromagnetic resonance with magnetic field modulation. Appl. Phys. Lett. 103, 172406 (2013).

- Mosendz, O. et al. Detection and quantification of inverse spin Hall effect from spin pumping in permalloy/normal metal bilayers. *Phys. Rev. B* 82, 214403 (2010).
- Garello, K. et al. Symmetry and magnitude of spin-orbit torques in ferromagnetic heterostructures. *Nat. Nanotech.* 8, 587–593 (2013).
- 23. Safranski, C. et al. Spin caloritronic nano-oscillator. Nat. Commun. 8, 117 (2017).
- Demidov, V. E. et al. Chemical potential of quasi-equilibrium magnon gas driven by pure spin current. Nat. Commun. 8, 1579 (2017).
- 25. Du, C. et al. Control and local measurement of the spin chemical potential in a magnetic insulator. *Science* **357**, 195–198 (2017).
- 26. Humphries, A. M. et al. Observation of spin-orbit effects with spin rotation symmetry. *Nat. Commun.* **8**, 911 (2017).
- Baek, S.-C. Spin currents and spin-orbit torques in ferromagnetic trilayers. Nat. Mater. 17, 509–513 (2018).
- Mann, M. & Beach, G. S. D. Reduction of in-plane field required for spin-orbit torque magnetization reversal by insertion of Au spacer in Pt/Au/ Co/Ni/Co/Ta. APL Mater. 5, 106104 (2017).
- Ryu, K.-S., Thomas, L., Yang, S.-H. & Parkin, S. Chiral spin torque at magnetic domain walls. *Nat. Nanotech.* 8, 527–533 (2013).
- Legrand, W. et al. Room-temperature current-induced generation and motion of sub-100 nm skyrmions. Nano Lett. 17, 2703–2712 (2017).

Acknowledgements

We thank M. Arora and E. Girt for discussion on the Co/Ni multilayer growth. Work on the deposition of the magnetic multilayers was supported as part of the Spins and Heat in Nanoscale Electronic Systems (SHINES), an Energy Frontier Research Centre funded by the US Department of Energy, Office of Basic Energy Sciences under Award no. DE-SC0012670. Nanowire device fabrication was supported by the US Department of Energy, Office of Basic Energy Sciences under Award no. DE-SC0014467. Spin torque oscillator development was supported by the National Science Foundation under Award no. DMR-1610146. Work on the variable-angle ST-FMR set-up development was supported by the National Science Foundation under Award no. EFMA-1641989. ST-FMR characterization was supported by the Army Research Office under Award no. W911NF-16-1-0472. Work on the absorptive FMR and spin pumping measurements was supported by the Defence Threat Reduction Agency under Award no. HDTRA1-16-1-0025. Work on experiment design and SOT analysis was supported by the National Science Foundation under Award no. ECCS-1708885.

Author contributions

E.A.M. deposited the magnetic multilayers, and performed the resistivity, absorptive FMR and spin pumping measurements. C.S. and E.A.M. fabricated the nanowire devices, and performed the ST-FMR and spin torque oscillator measurements. I.N.K. designed the experiment and performed the SOT analysis. All the authors analysed the data and co-wrote the paper.

Competing interests

The authors declare no competing interests.

Additional information

Supplementary information is available for this paper at https://doi.org/10.1038/s41565-018-0282-0.

Reprints and permissions information is available at www.nature.com/reprints.

Correspondence and requests for materials should be addressed to I.N.K.

Publisher's note: Springer Nature remains neutral with regard to jurisdictional claims in published maps and institutional affiliations.

© The Author(s), under exclusive licence to Springer Nature Limited 2018

NATURE NANOTECHNOLOGY LETTERS

Methods

Sample preparation. The multilayers were deposited by d.c. magnetron sputtering on $Al_2O_3(0001)$ substrates in 2 mtorr of Ar process gas. The highly resistive Ta seed and cap layers were employed to reduce the roughness and to prevent oxidation of the multilayers, respectively. The multilayers were patterned into $40\text{--}50\,\text{nm}$ wide, $40\,\mu\text{m}$ long nanowires via electron-beam lithography using negative resist HSQ and subsequent ion mill etching. The electrical leads to the nanowire were patterned via electron-beam lithography using a methyl methacrylate/poly(methyl methacrylate) positive resist bilayer followed by the sputter deposition of Ta(5 nm)/Au(40 nm)/ Ta(5 nm) and liftoff. The spacing between the leads defined an active region $80\text{--}190\,\text{nm}$ long in the central part of the nanowire.

ST-FMR. The application of a microwave current to the sample excites the magnetization and sample resistance oscillations at the frequency of the drive. These resistance oscillations mix with the applied microwave current and generate a rectified voltage $V_{\rm mix}$. Resonances in $V_{\rm mix}$ were observed at the frequency and field values that corresponded to the spin wave eigenmodes of

the system. To improve the sensitivity of the method, we modulated the applied magnetic field and measured $\tilde{V}_{\rm mix}(H) \approx {\rm d}V_{\rm mix}(H)$. To determine the resonance field and linewidth ΔH of the spin wave modes, we fit the resonances in $\tilde{V}_{\rm mix}(H)$ by the magnetic field derivative of the sum of Lorentzian and anti-Lorentzian functions 20 .

Microwave emission measurements. The microwave power emitted from the nanowire was detected using a spectrum analyser. A direct current was applied to the sample through the d.c. port of a bias tee. The microwave port of the tee was connected to a low noise microwave amplifier with a gain of 45 dB, and the signal was then recorded by the spectrum analyser.

Data availability

All data supporting the findings of this study are available within the article and the Supplementary Information and are available at the University of California Data Repository at https://doi.org/10.15146/R3H09M. All the data are available from the authors on request.